Journal of Physics B: Atomic, Molecular and Optical Physics

PAPER

Photoemission from hybrid states of $Cl@C_{60}$ before and after a stabilizing charge transfer

To cite this article: Dakota Shields *et al* 2020 *J. Phys. B: At. Mol. Opt. Phys.* **53** 125101

IOP Publishing Journal of Physics B: Atomic, Molecular and Optical Physics
J. Phys. B: At. Mol. Opt. Phys. **53** (2020) 125101 (8pp) https://doi.org/10.1088/1361-6455/ab82df

Photoemission from hybrid states of Cl@C_{60} before and after a stabilizing charge transfer

Dakota Shields[1], Ruma De[1], Mohamed E Madjet[2], Steven T Manson[3] and Himadri S Chakraborty[1,4]

[1] Department of Natural Sciences, D. L. Hubbard Center for Innovation, Northwest Missouri State University, Maryville, MO 64468, United States of America
[2] Qatar Environment and Energy Research Institute, Hamad Bin Khalifa University, P.O. Box 34110, Doha, Qatar
[3] Department of Physics and Astronomy, GA State University, Atlanta, GA, United States of America

E-mail: himadri@nwmissouri.edu

Received 6 January 2020, revised 17 February 2020
Accepted for publication 24 March 2020
Published 27 May 2020

Abstract

Photoionization calculations of the endofullerene molecule Cl@C_{60} with an open-shell chlorine atom are performed in the linear response density functional theory based on a spherical jellium model of C_{60}. Cross sections for atom–fullerene hybrid photoemission studied show the effects of the hybridization symmetry, the giant plasmon and the molecular cavity. Comparisons with the results of Ar@C_{60} provide insights into the role of a shell-closing electron and its influence on the dynamics. The results for Cl@C_{60} are further compared with those of a more stable configuration that results after a C_{60} electron transfers to Cl forming Cl^-@C_{60}^+. This comparison reveals noticeable differences in the ionization properties of the antibonding hybrid state while the bonding hybrid remains nearly unaltered showing a magnification covering the entire giant plasmon energy range. These predictions should raise interest in probing the molecular configuration using photoelectron spectroscopy.

Keywords: photoionization, endofullerenes, hybridization

(Some figures may appear in colour only in the online journal)

1. Introduction

Significant success in the synthesis of endofullerene molecules—systems of an atom or a smaller molecule incarcerated within the fullerene cage [1]—has spawned a series of experiments [2–4] using merged beam techniques at the Berkeley Advanced Light Source. The experiments accessed photoionization properties of these materials in gas phase. In addition, endofullerenes, being natural entrapment of atoms, have led to a series of theoretical studies of the effects of ionizing radiation on these systems, i.e., photoionization [5, 6]. Such fundamental spectroscopic knowledge is particularly useful due to a broad horizon of applied importance of these materials in, namely, (i) solid state quantum computations [7, 8], (ii) improving the superconducting ability of materials [9], (iii) biomedical fields [10], (iv) contrast-enhancement research for magnetic resonance imaging (MRI), (v) improving organic photovoltaic devices [11], and even in (vi) astrophysics [12].

Endofullerenes confining open-shell atoms have potential applied interests of rather exotic nature [13]. For instance, N@C_{60} has attracted interest due to its uniquely long spin relaxation times driven by the confinement [14]. Electron paramagnetic resonance study [15] of P@C_{60} has shown enhancement in hyperfine coupling of the phosphorous' unpaired electrons with its nucleus which is attributed to the admixture of

[4] Author to whom any correspondence should be addressed.

excited states acquiring angular momentum from the cage. In contrast, the hyperfine interaction between the positively-charged muon and the unpaired electrons in the muonium atom in C_{60}, relative to free muonium, is predicted to diminish from the confinement [16]. These discoveries render particular relevance to study open-shell atomic endofullerenes, including assessing the spectroscopy of their more stable configurations resulting from electron transfers to atomic vacancies.

One unique phenomenon that ubiquitously occurs across endofullerene systems is the emergence of atom–fullerene ground state orbital hybridization. This entails the formation of symmetric (bonding) and antisymmetric (antibonding) hybrid states as the eigenstates of the whole system from the mixing of an atomic and a fullerene orbital of identical angular momentum symmetry. A number of our previous studies have predicted such hybrid states in various endofullerenes and their broad spectrum of photoionization properties [17–21]. It is therefore of particular value to scrutinize the sensitivity of the hybridization and the photoemission dynamics of these hybrid states via gentle changes of configuration features by, for instance, comparing the effects of confinement upon successive atoms in the periodic table. It is important to note that while the simple static annular square well (ASW) model potential is often useful [5, 22], the model does not include C_{60} electrons; consequently, the possibility of hybridization is omitted in ASW calculations. Besides, the absence of electrons in the ASW model vastly limits both ground-state and dynamical electron correlations.

A prototype case that we examine here is the hybrid level photoionization of $Cl@C_{60}$ versus $Ar@C_{60}$; Cl has just one electron less than Ar in the outer 3p shell and an atomic number lower by one. Closed-shell Ar, being chemically inert, almost certainly locates at the center of the spherical C_{60}. We treat the barely open-shell Cl also within the spherical geometry so as to retain the same spherical calculation as was done for the Ar case. We then consider a system of $Cl^-@C_{60}{}^+$ produced by the transfer of a C_{60} electron to fill in the Cl hole. This configuration likely attains more stability by forming closed-shell Cl^-. There has been experimental evidence, based on laser desorption mass spectroscopy, of C_{60} with a single Cl^- inside [23]. While it is expected that the polarization interaction of the ion can induce some offset in its position from the center of C_{60}, a density functional theory calculation with Born–Oppenheimer molecular dynamics indicates that this offset is quite small within neutral C_{60} [24]. Earlier studies showed only small effects of the cage polarization except very close to the ionization threshold [25]. Likewise, a relatively weak effect on the process from a small offset of the atomic location was predicted [26]. Therefore, we treat $Cl^-@C_{60}{}^+$ assuming spherical geometry as well. We then compare the hybrid photoionization of this new configuration with $Cl@C_{60}$. Ultimately, the general comparison among these three endofullerene systems unfolds the delicate dependence of the hybridization and resulting photoionization cross sections on a shell-closing electron as well as on an electron transfer from the cage to the atom.

2. Brief description of theory

The details of the theory are described in reference [18]. Choosing the photon polarization along the z-axis, the photoionization dipole transition cross section in a linear response approximation of time-dependent density functional theory is given by

$$\sigma_{n\ell\to k\ell'} \sim |\langle\psi_{\mathbf{k}\ell'}|z+\delta V|\phi_{n\ell}\rangle|^2. \tag{1}$$

Here $\mathbf{k}$ is the momentum of the continuum electron, z is the one-body dipole operator, ϕ_{nl} is the single electron bound wavefunction of the target level, and $\psi_{\mathbf{k}l'}$ is the respective outgoing dipole-allowed continuum wavefunction, with $l' = l \pm 1$. δV represents the complex induced potential that accounts for electron correlations within the linear response framework.

We model the bound and continuum states self-consistently using the independent particle local density approximation (LDA) modified by van Leeuwen–Baerends (LB) exchange–correlation functional [27]. The jellium potentials, $V_{\rm jel}(\mathbf{r})$, representing 60 C^{4+} ions for C_{60} is constructed by smearing the total positive charge over a spherical shell with known molecular radius $R = 3.54$ Å (6.70 a.u.) [28] and thickness Δ. A constant pseudopotential $\overline{v}$ is added to $V_{\rm jel}$ for quantitative accuracy. The Kohn–Sham equations for the system of 240 electrons (four valence $2s^22p^2$ electrons from each carbon atom), *plus* all electrons of the central atom with atomic number ζ, are then solved in the LDA + LB potential

$$V_{\rm LDA+LB}(\mathbf{r}) = -\frac{\zeta}{r} + V_{\rm jel}(\mathbf{r}) + \int d\mathbf{r}'\frac{\rho(\mathbf{r}')}{|\mathbf{r}-\mathbf{r}'|} + V_{\rm XC}[\rho(\mathbf{r})], \tag{2}$$

to obtain the bound and continuum orbitals in equation (1) self-consistently as described in reference [18]. Besides the LDA term, equation (2) also includes the LB exchange–correlation functional in $V_{\rm XC}$ involving the gradient of the electron density in the scheme described earlier [29]. This approach provides an accurate asymptotic description of the ground state potential. The values of Δ and $\overline{v}$ and are determined both by requiring charge neutrality and obtaining the experimental value [30] of the first ionization threshold of C_{60}. $\Delta = 1.30$ Å (2.46 a.u.) thus obtained closely agree with that extracted from measurements [28]. $\overline{v}$ was found to be 12.1 eV. Obviously, omitting either ζ/r or $V_{\rm jel}$ in equation (2) produces, respectively, the empty C_{60} and the free atomic results.

We remark that treating open-shell, thus non-spherical, 3p orbital density of Cl in a spherical frame may produce inaccuracies in Hartree–Fock type methods that treat the non-local exchange exactly [31]. In the density functional model as in the current study, on the other hand, one may adjust the parameters of the functional, or use a different functional, to force accurate ground state properties [32]. However, we could not find a unique set of parameter values of our LB functional to work for both free Cl and empty C_{60}. Therefore, we have used the set, that is successful for C_{60}, for the endohedral composite-systems as well. But these values overestimate Cl ionization potential of NIST database [33] by about 7%. They further produce an electron affinity of −4.15 eV as opposed to the measured value of −3.6 eV [34], even though Cl^- has a closed-shell spherical 3p shell. But these

small inaccuracies should not take away much from the main results of this study which explores the dominant effects of C_{60}.

The time-dependent (TD) LDA + LB-derived $z + \delta V(\mathbf{r})$ in equation (1) is proportional to the induced changes in the electron density as a function of the photon frequency ω [35]. This change is

$$\delta\rho(\mathbf{r}';\omega) = \int \chi(\mathbf{r},\mathbf{r}';\omega) z d\mathbf{r}, \tag{3}$$

where the full susceptibility, χ, builds the dynamical correlation from the independent-particle LDA + LB susceptibilities

$$\chi^0(\mathbf{r},\mathbf{r}';\omega) = \sum_{nl}^{\text{occ}} \phi^*_{nl}(\mathbf{r})\phi_{nl}(\mathbf{r}')\, G(\mathbf{r},\mathbf{r}';\epsilon_{nl}+\omega) + \sum_{nl}^{\text{occ}} \phi_{nl}(\mathbf{r})\phi^*_{nl}(\mathbf{r}')\, G^*(\mathbf{r},\mathbf{r}';\epsilon_{nl}-\omega) \tag{4}$$

through the matrix equation $\chi = \chi^0[1-(\partial V/\partial\rho)\chi^0]^{-1}$ involving the variation of the ground-state potential V with respect to the ground-state density ρ. The radial components of the full Green's functions in equation (4) are constructed with the regular (f_L) and irregular (g_L) solutions of the homogeneous radial equation

$$\left(\frac{1}{r^2}\frac{\partial}{\partial r}r^2\frac{\partial}{\partial r} - \frac{L(L+1)}{r^2} - V_{\text{LDA+LB}} + E\right) f_L(g_L)(r;E) = 0 \tag{5}$$

as

$$G_L(r,r';E) = \frac{2 f_L(r_<;E) h_L(r_>;E)}{W[f_L,h_L]} \tag{6}$$

where W represents the Wronskian and $h_L = g_L + i f_L$ and E is the photoelectron energy. Obviously, TD(LDA + LB) thus includes the dynamical many-electron correlation by improving upon the mean-field LDA + LB description.

3. Results and discussion

3.1. Cl@C_{60} versus Ar@C_{60}

3.1.1. Ground state atom–C_{60} hybridization: In an endofullerene system, an eigenstate of the free atomic Hamiltonian can admix with an eigenstate of the empty C_{60} Hamiltonian of the same angular momentum symmetry to produce hybrid states which are eigenstates of the combined system. Thus, ground state LDA + LB results for Cl@C_{60} reveal hybridization between valence 3pCl and a deeper 2pC_{60} state (2p state of a jellium C_{60}), both of the same angular character, which jointly produce symmetrically and antisymmetrically combined states of Cl@C_{60} that can be written as,

$$|\text{Cl}+\text{C}_{60}\rangle = |\phi_+\rangle = \sqrt{\alpha}|\phi_{3\text{p Cl}}\rangle + \sqrt{1-\alpha}|\phi_{2\text{pC}_{60}}\rangle \tag{7a}$$

$$|\text{Cl}-\text{C}_{60}\rangle = |\phi_-\rangle = \sqrt{1-\alpha}|\phi_{3\text{p Cl}}\rangle - \sqrt{\alpha}|\phi_{2\text{pC}_{60}}\rangle \tag{7b}$$

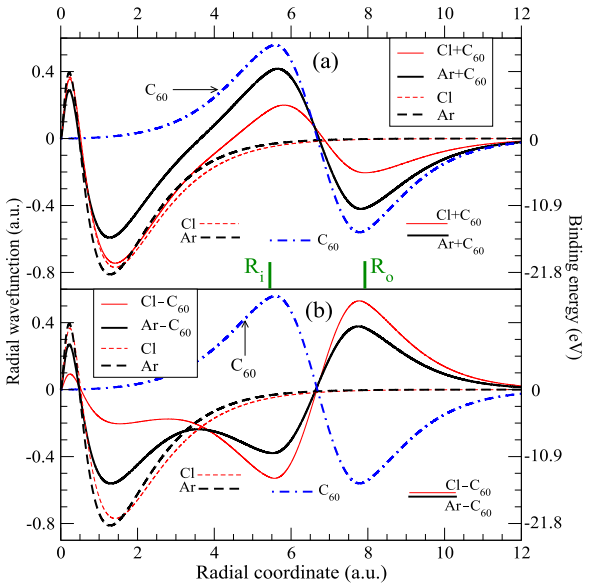

Figure 1. LDA + LB radial symmetric (a) and antisymmetric (b) wavefunctions of Cl@C_{60} versus Ar@C_{60}. For both the molecules the 3p level of the free atom hybridizes with the 2p level of free C_{60}; wavefunctions of these free systems are also displayed. Relevant binding energies in eV (scaled in opposite y-axis) are also graphed to aid the discussion in the text. The inner (R_i) and outer (R_o) radii of the C_{60} shell are shown on panel (a).

where the fraction α is the mixing parameter that renders the states orthonormal. Note that, we use the hydrogenic Coulomb notation of labeling for the atom and the standard harmonic oscillator notion for C_{60}. In figure 1, the radial components of these wavefunctions are shown and compared with the corresponding hybrid wavefunctions of Ar@C_{60}. Due to opposite mixing signs in equations (7a) versus (7b), the symmetric hybrid shows a radial oscillation at the shell region which is *in-phase* with that of 2pC_{60}, while it is *out-of-phase* for the antisymmetric hybrid. From a perturbation theory viewpoint, the strength of this mixing is proportional directly to the overlap of the participating (free) orbitals and inversely to the separation of their binding energies. As figure 1 indicates, the energy of 3pAr is extremely close to that of 2pC_{60}, while 3pCl moves a bit higher, leading to a stronger mixing with a value of α close to about 0.5 (equal share of atom–fullerene character) for Ar@C_{60}. This result is different from a weaker hybridization found in earlier LDA calculations of Ar@C_{60} [36, 37] which did not utilize the gradient corrected LB exchange–correlation functional of the current study that goes beyond LDA.

A somewhat reduced hybridization in Cl@C_{60} with a greater value of α thus implies enhanced Cl and enhanced C_{60} characters, respectively, for the symmetric and antisymmetric states (figure 1). This occurs in spite of a slightly increased wavefunction overlap due to a small displacement of 3pCl wavefunction toward the shell from that of 3pAr. Also note that the resulting symmetric hybrids of the systems are more separated energetically than the antisymmetric hybrids.

3.1.2. Photoionization of hybrid levels. Cross sections calculated at the correlated TD(LDA + LB) level for the hybrid

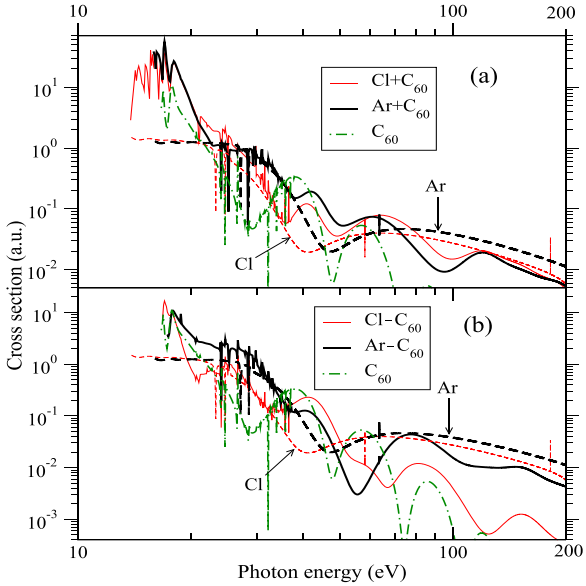

Figure 2. TD(LDA + LB) photoionization cross sections of symmetric (a) and antisymmetric (b) levels of Cl@C_{60} compared to Ar@C_{60}. Cross sections for 3p of free Cl and free Ar, and for 2p of empty C_{60} are also plotted for comparisons.

states of Cl@C_{60} and Ar@C_{60} are presented in figure 2 as a function of the photon energy. (Several narrow resonances are due to the many autoionization resonance channels that exist in the endofullerenes due to levels in the fullerene molecule that are not there in free atom.) Comparing these with 3p of free Cl and Ar indicates plasmon driven enhancements at low energies [20, 36]. This enhancement is significantly stronger for symmetric photoemission than the antisymmetric one. In the framework of interchannel coupling due to Fano, the correlation-modified [TD(LDA + LB)] matrix element of the photoionization of X ±C_{60}, X being Cl or Ar, can be written as [20],

$$\mathcal{M}_{\pm}(E)=\mathcal{D}_{\pm}(E)+\sum_{n\ell}\int dE'\,\frac{\langle\psi_{n\ell}(E')|\frac{1}{|\mathbf{r}_{\pm}-\mathbf{r}_{n\ell}|}|\psi_{\pm}(E)\rangle}{E-E'}\mathcal{D}_{n\ell}(E') \tag{8}$$

in which the single electron (LDA + LB) matrix element is

$$\mathcal{D}_{\pm}(E)=\langle ks(d)|z|\phi_{\pm}\rangle \tag{9}$$

and $|\psi_{nl}\rangle$ in the interchannel coupling integral is the (continuum) wavefunction of the $n\ell \to k\ell'$ channel. Taking the hybridization into account, the channel wavefunctions in equation (8) become

$$|\psi_{+}\rangle=\sqrt{\alpha}|\psi_{3\mathrm{p\,X}}\rangle+\sqrt{1-\alpha}|\psi_{2\mathrm{pC_{60}}}\rangle \tag{10a}$$

$$|\psi_{-}\rangle=\sqrt{1-\alpha}|\psi_{3\mathrm{p\,X}}\rangle-\sqrt{\alpha}|\psi_{2\mathrm{pC_{60}}}\rangle. \tag{10b}$$

Substituting equations (7a) and (7b), but for a general X, and equations (10a) and (10b) in equation (8), and noting that the overlap between a pure X and a pure C_{60} bound state is negligible, we separate the atomic and fullerene contributions to the integral to get the TD(LDA + LB) matrix element for X ±C_{60} levels as,

$$\mathcal{M}_{+}(E)=\sqrt{\alpha}\mathcal{M}_{3\mathrm{p\,X}}(E)+\sqrt{1-\alpha}\mathcal{M}_{2\mathrm{pC_{60}}}(E) \tag{11a}$$

$$\mathcal{M}_{-}(E)=\sqrt{1-\alpha}\mathcal{M}_{3\mathrm{p\,X}}(E)-\sqrt{\alpha}\mathcal{M}_{2\mathrm{pC_{60}}}(E), \tag{11b}$$

where the second terms on the right-hand side are responsible for the plasmonic enhancements at the lower energies, as seen in figure 2. Obviously, $|\mathcal{M}_{2\mathrm{pC_{60}}}|^2$ will produce the 2p cross section of empty C_{60} which we also include in figure 2 for comparison. As seen, while the cross sections for the symmetric hybrid of both endohedral systems enhance far more than that of $2pC_{60}$ at plasmon energies, they are comparable for the antisymmetric hybrids. Writing the atomic and C_{60} contributions in equations (11a) and (11b) respectively as complex quantities $X_r + iX_i$ and $C_r + iC_i$ (subscript r and i for the real and imaginary part), and recalling that the cross section σ is proportional to the square modulus of the matrix element, we can express the cross sections as,

$$\sigma_{+}(E)\sim(\sqrt{\alpha}X_r+\sqrt{1-\alpha}C_r)^2+(\sqrt{\alpha}X_i+\sqrt{1-\alpha}C_i)^2 \tag{12a}$$

$$\sigma_{-}(E)\sim(\sqrt{1-\alpha}X_r-\sqrt{\alpha}C_r)^2+(\sqrt{1-\alpha}X_i-\sqrt{\alpha}C_i)^2. \tag{12b}$$

Evidently, the enhancement of the symmetric state cross section, equation (12a), involving the sum of real and imaginary components, will be universally larger than that of the antisymmetric state which include their differences. Indeed, this is seen for both Cl@C_{60} and Ar@C_{60} in figure 2 and a direct consequence of the in-phase versus out-of-phase radial oscillation of the hybrid wavefunctions at C_{60} shell (figure 1). However, the detailed similarities and differences of enhanced cross section between two systems must depend on their respective values of α in a rather complicated way that involves the interferences between the atomic and the C_{60} components of the matrix elements in equations (12a) and (12b). We note that while this enhancement is of a comparable size for the symmetric states of both systems in figure 2(a), it is significantly weaker for antisymmetric Cl–C_{60} compared to Ar–C_{60} (figure 2(b)). The situation further complicates from the effect of lowering binding energies of Cl@C_{60} hybrid levels as is discussed in section 3.2 below.

As the plasmonic effect weakens with increasing energy, the cross sections largely follow their free atom curves, as seen in figure 2. Cooper minimum-like structures develop [38] around 50 eV on both the symmetric curves with the minimum of Cl@C_{60} being deeper due to its higher atomic character. Note that the Cooper minima in 3p cross sections for free atoms are clearly visible in figure 2. In any case, such minima also show up around 60 eV for antisymmetric emissions where the structure for Cl@C_{60} is very weak because of its weaker atomic character.

Above these energies the cross sections oscillate as a consequence of a well-known multipath interference mechanism [39] due to the cavity structure of C_{60} which was modeled

earlier in detail in reference [40]. At such high energies the interchannel coupling in equation (8) vanishes to simplify equations (11a) and (11b) to,

$$\mathcal{D}_{+}(E) = \sqrt{\alpha}\mathcal{D}_{3\mathrm{p\,X}}(E) + \sqrt{1-\alpha}\mathcal{D}_{2\mathrm{pC_{60}}}(E) \tag{13a}$$

$$\mathcal{D}_{-}(E) = \sqrt{1-\alpha}\mathcal{D}_{3\mathrm{p\,X}}(E) - \sqrt{\alpha}\mathcal{D}_{2\mathrm{pC_{60}}}(E). \tag{13b}$$

The multipath interference model is based on the following mechanism. The matrix element $\mathcal{D}$ can generally be isolated in to two components, one arising from the atomic region and other from the C_{60} shell region, and can be written down respectively as follows [40]

$$\mathcal{D}_{\mathrm{X}} \sim \mathcal{D}^{\,\mathrm{atom}}(k) + A^{\,\mathrm{refl}}(k)\left[\mathrm{e}^{-ikD_{\mathrm{o}}}\mathrm{e}^{-iV_0\frac{2\Delta}{k}} - \mathrm{e}^{-ikD_{\mathrm{i}}}\right] \tag{14a}$$

$$\mathcal{D}_{C} \sim A^{\,\mathrm{shell}}(k)\mathrm{e}^{-i\frac{V_0}{k}}\left[a_{\mathrm{i}}\mathrm{e}^{-ikR_{\mathrm{i}}} - a_{\mathrm{o}}\mathrm{e}^{-ikR_{\mathrm{o}}}\right], \tag{14b}$$

where the photoelectron momentum $k = \sqrt{2(E-\epsilon_{\pm})}$ in atomic units, a_{i} and a_{o} are the values of $\phi_{\pm}$ at the inner and outer radii R_{i} and R_{o} of C_{60}, and V_0 is the average depth of the shell potential. In equation (14a), $\mathcal{D}^{\,\mathrm{atom}}$ represents the direct ionization amplitude from the atomic region. The second term in this equation embodies the reflection of this outgoing photoelectron wave from both inner and outer surfaces of the shell. Quantitatively, this induces oscillations as a function of the photoelectron momentum with amplitude A^{refl} and frequencies related to D_{i} and D_{o}, the inner and outer diameters of the shell. The direct and the reflected parts coherently interfere in the cross section. Since, obviously, A^{refl} is proportional to $\mathcal{D}^{\,\mathrm{atom}}$, the larger the atomic component of a hybrid wavefunction, the stronger is the reflection and the higher is the chances that the oscillations occur about the free atom result. This is exactly what is seen for the high energy cross section of Cl + C_{60} in figure 2(a). On the other hand, equation (14b), the portion of the overlap integral from the shell region, produces two localized emissions from shell edges, where the maximum ionizing forces become available due to rapid variations of the shell potential there. Such a diffraction-type effect translates into another oscillation in frequencies related to R_{i} and R_{o}. This part will also add to coherent interference in the cross section and will dominate if a hybrid level has a stronger C_{60} character, like for Cl–C_{60}. Indeed, the oscillations in the cross section of Cl–C_{60} intensify at higher energies while the average value fall significantly lower than free 3pCl (figure 2(b)). For the Ar@C_{60} hybrids, however, due to their almost equal share of atom–C_{60} character (figure 1), the strength of high-energy cross sections are comparable, somewhat below 3pAr, but the differences in the details of their shapes again owe to the interference between reflective and diffractive emissions described above. We further note in figure 2 that for the pure $2pC_{60}$ shell, which predominantly emits by the diffraction mechanism of equation (14b) at high energies, the result shows sharper oscillations with very rapid fall-off due to the absence of any atomic type steady emission [41].

3.2. Cl@C_{60} versus Cl^-@C_{60}^+

A reactive Cl atom is very likely to capture an electron from C_{60} which will likely bring the compound to a more stable configuration Cl^-@C_{60}^+. If an electron transitions from the highest occupied (HOMO) level of C_{60} of binding energy −7.52 eV to 3pCl level of electron affinity −4.15 eV, then the resulting configuration with the hole in HOMO will have the minimum total energy and, therefore, will be the ground state configuration for Cl^-@C_{60}^+. This does not even take into account the extra binding associated with the electrostatic Coulomb attraction between Cl^- and C_{60}^+. Despite the electron affinity of Cl being less than the ionization potential of C_{60} (see above), this extra binding is what that will enable the ionic compound to bind. Therefore, this ground state configuration of Cl^-@C_{60}^+ should be stable and abundantly formed.

We further note that if Cl@C_{60} is already at the lowest energy, then a C_{60} electron relocating to Cl will raise the energy of the molecule; the latter being stable will, thus, form a metastable configuration. On the other hand, the realistic ground state of the compound may as well be a mixture of Cl@C_{60} and Cl^-@C_{60}^+ with more of the latter's character. However, the comparison of the photoionization properties between these two diabatically unique configurations, as carried out in the present study, is of interest to understand the interplay between the two modes. Moreover, the similarities and variations of these properties based on two distinct configurations suggest the experimental need to access the real system via photoelectron spectroscopy [28], especially of the photoelectrons emitted from the atom–fullerene hybrid levels.

The excited state configurations of Cl^-@C_{60}^+ will be formed going higher in total energy as the transferred electron originates from gradually deeper states of C_{60}, ignoring the relaxation of the hole. For an empty C_{60}^+, our LDA + LB ground state structure is insensitive to the location of the hole among the molecular levels which is not too surprising for a cloud of 240 delocalized electrons. Likewise, for the complex Cl^-@C_{60}^+ the LDA + LB energies and wavefunctions of all pure C_{60} and hybrid states are found independent of which C_{60} orbital the hole is situated at. This fact makes our current result rather robust. Furthermore, the energies and wavefunctions for pure C_{60} levels of the compound remain practically identical to those of empty C_{60}, and therefore of little interest. However, the hybridization between $3pCl^-$ and $2pC_{60}^+$ is somewhat modified from that in Cl@C_{60}, or, in other words, between after and before the electron makes a transition, as we describe below. Yet it is found that the hybridization in Cl^-@C_{60}^+ is still insensitive to the C_{60} level the electron transitions from, that is the location of the hole. Therefore, our results presented here are robust being free of a specific choice of the hole level. On the other hand, we calculate Cl levels in Cl^-@C_{60}^+ to have higher binding energies than the Cl levels of Cl@C_{60} to match the trend that it takes about 4.15 eV to remove a 3p electron from Cl^- to produce Cl.

The hybridization in Cl^-@C_{60}^+ is compared to that in Cl@C_{60} in figure 3. Note that for Cl^-@C_{60}^+ the

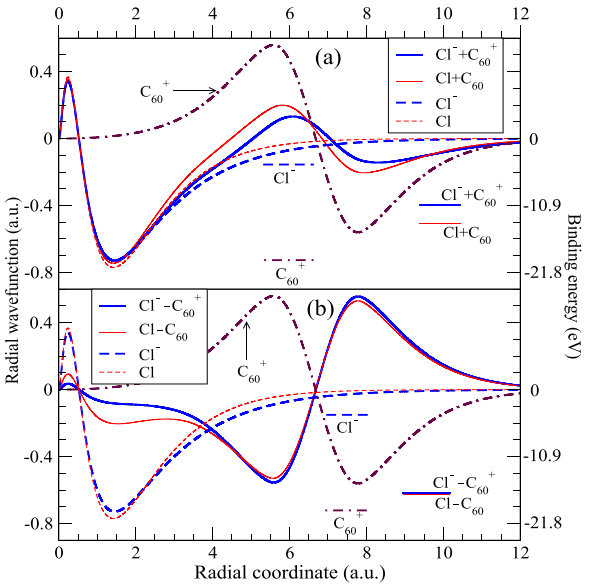

Figure 3. Same as figure 1 but for Cl@C_{60} in comparison with a more stable configuration Cl^-@C_{60}^+ of the molecule. Participating wavefunctions of the free systems Cl, Cl^- and C_{60}^+, and relevant binding energies in eV are included.

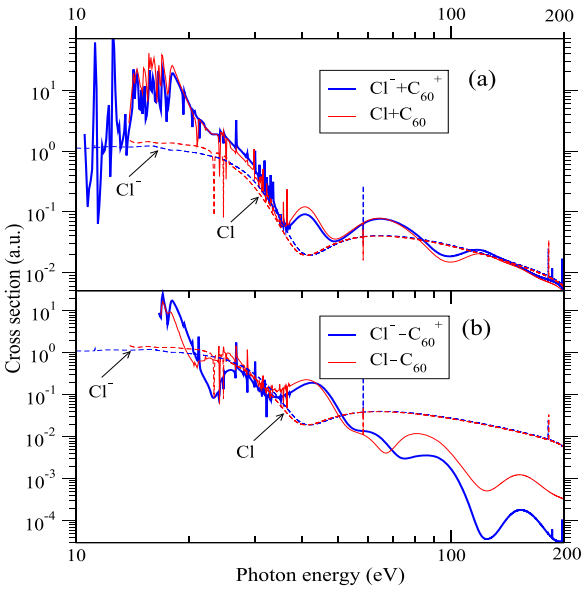

Figure 4. Same as figure 2 but for Cl@C_{60} versus Cl^-@C_{60}^+ configuration. TD(LDA + LB) cross sections for 3p of free Cl and free Cl^- are also shown.

participating free levels 3pCl^- and 2p@C_{60}^+ are significantly apart from each other (figure 3), the former becoming quite shallower and the latter becoming deeper compared to their counterparts in Cl@C_{60} (figure 1). This strongly disfavors the hybridization. Conversely, as also seen in figure 3, the radial wavefunction of 3pCl^- extends more radially outward than 3pCl to increase its overlap with 2pC_{60}^+ which favors the hybridization. In the tug-of-war between these two effects, the former wins resulting in some modification of hybridization for Cl^-@C_{60}^+ configuration as displayed in figure 3. It is seen that the atomic character stays unchanged, but the C_{60} character weakens at the shell for the symmetric hybrid, while the reverse is true for the antisymmetric hybrid. Comparing the energy of the hybrid levels, the symmetric hybrid moves energetically higher (figure 3(a)) while the antisymmetric hybrids barely separate (figure 3(b)) as a result of the charge transfer. And this modified hybridization affects the resulting photoionization cross sections.

Figure 4 compares the TD(LDA + LB) cross sections for photoionization from hybrid levels of Cl^-@C_{60}^+ with Cl@C_{60}. Note that even though there is a slight modification in hybridization (figure 3) post electron transfer, the cross section of the symmetric level (figure 4(a)) is hardly modified, except that Cl^- + C_{60}^+ starts at a lower photon energy due to the reduction of its binding energy. To be more precise, some reduction in the amplitude of the structure of Cl^- + C_{60}^+ wavefunction (figure 3(a)) in the shell region results in little effect on the cross section. In the energy region of the plasmon, this can be understood in general from the interchannel coupling contribution of the matrix element in equation (8). Specifically, this term in part embodies the overlaps of the 'fractional' ionization channel emanating from the shell region of the symmetric hybrid with all C_{60} channels which are accounted for in $\mathcal{M}_{2pC_{60}}$ in equation (12a). The channel overlap includes both the overlap between the bound and the continuum wavefunctions. While the reduction of the structure in Cl^- + C_{60}^+ radial wave noted above lowers the aggregated strength of bound overlaps, the continuum overlaps will be slightly favored due to the following reason. A continuum overlap is more efficient at higher photoelectron momenta k, since differences between the momenta due to different level energies reduce enabling the continuum waves to oscillate progressively in phase with each other. Therefore, the Cl^- + C_{60}^+ state opening at a lower photon energy benefits continuum overlaps to cause its net increase. This gain must be compensating the loss due to weakening hybridization to affect practically no change in the symmetric hybrid level cross section (figure 4(a)) after the electron transfers. Note that the term $\mathcal{M}_{3p\,X}$ in equation (12a) has no effect here due to about the same atomic character of hybrid wavefunctions before and after the electron switches locations. For the higher energy emission of this hybrid (figure 4(a)), a rather miniscule weakening of the multipath oscillations following the electron transfer traces to the reduction of its C_{60} character that slightly reduces the collateral emission in equations (14a) and (14b), while keeping the reflective emission unchanged. The strong atomic character of this hybrid, which remains unchanged in spite of the electron transition, keeps the average strength of both cross sections close to 3p of Cl and Cl^- which are practically equal at these energies.

Differences between the cross sections of antisymmetric hybrid states of Cl^-@C_{60}^+ and Cl@C_{60}, shown in figure 4(b), are rather strong. The differences at plasmonic energies up to 40 eV are due to the reduction of the atomic character (figure 3(b)), particularly via the interference effects illustrated in equation (12b). Note that since the binding energies of this hybrid state suffer a very little change upon the charge transfer, the continuum overlap effect described above does not apply.

However, at higher energies, 80 eV and above, the difference in cross sections grows progressively stronger. This must be due a cumulative effect of the reduction of the atomic component of direct ionization, as a result of the reduced atomic character in $Cl^- - C_{60}{}^+$, the subsequent reduction of reflective amplitude in equations (14a) and (14b), and the interference between them. To this end, even after the molecule evolves to a stable configuration $Cl^-@C_{60}{}^+$, the strong plasmonic magnification of the emission from the symmetric hybrid remains, but the high energy response of the antisymmetric state substantially changes. More generally, comparing results of figure 2 with 4, we note a slow trend of modification for the symmetric hybrid cross sections from $Ar@C_{60}$ to $Cl@C_{60}$ to $Cl^-@C_{60}{}^+$, while the change is rather dramatic along this sequence for the antisymmetric level. Finally, we note from equations (14a) and (14b) that for a possible small offset of Cl or Cl^- in the cage, the multipath interference oscillations will somewhat weaken from a dephasing effect, since the distance, the effective radius (R), of the atom to the cage will slightly vary from different directions.

4. Conclusions

Using a fairly successful methodology of the time-dependent local density approximation based on a spherical jellium modeling of C_{60}'s ion core, we compute the photoemission cross sections of the atom–fullerene hybrid levels of $Cl@C_{60}$. A comparison of the results with those of $Ar@C_{60}$ probes the modification effects of a shell-closing electron on the properties of these hybrid photoemissions. However, $Cl@C_{60}$ must be an unstable system and will likely induce an electron transfer from C_{60} to Cl to reach a more stable configuration. We compared the results between these two configurations of Cl endofullerenes as well to assess the effects of this electron transition on the hybrid photodynamics. Thus, in general, tuning the configuration gently along the sequence of $Ar@C_{60}$ to $Cl@C_{60}$ to $Cl^-@C_{60}{}^+$, a systematic evolution of the ionizing response of hybrid states is uncovered. A strong magnification of the low energy emission of the symmetric hybrid over the entire giant plasmon resonance region and an enhanced multipath interference effects for the high energy antisymmetric hybrid are the most robust features in our study. In specific, however, noticeable differences in the properties of the antibonding hybrid state ionization of $Cl@C_{60}$ versus $Cl^-@C_{60}{}^+$ are predicted, while the bonding hybrid remains nearly unaltered. This is the first study of the photoionization properties of a halogen endofullerene to the best of our knowledge. Like for any level of a complex target, the emission cross sections of the hybrid levels reported in this study can be experimentally accessed by conventional photoelectron spectroscopy techniques. This may open a direction to probe the ground and metastable excited configurations of halogen endofullerenes where an internal electron transition is possible.

Acknowledgments

The research is supported by the US National Science Foundation Grant No. PHY-1806206 (HSC) and the US Department of Energy, Office of Science, Basic Energy Sciences, under award DE-FG02-03ER15428 (STM).

ORCID iDs

Steven T Manson https://orcid.org/0000-0002-7072-4122
Himadri S Chakraborty https://orcid.org/0000-0001-5758-6418

References

[1] Popov A A, Yang S and Dunsch L 2013 Endohedral fullerenes *Chem. Rev.* **113** 5989
[2] Müller A, Schippers S, Habibi M, Esteves D, Wang J C, Phaneuf R A, Kilcoyne A L D, Aguilar A and Dunsch L 2008 Significant redistribution of Ce 4d oscillator strength observed in photoionization of endohedral $Ce@C_{82}^+$ ions *Phys. Rev. Lett.* **101** 133001
[3] Kilcoyne A L D *et al* 2010 Confinement resonances in photoionization of $Xe@C_{60}{}^+$ *Phys. Rev. Lett.* **105** 213001
[4] Phaneuf R A *et al* 2013 Probing confinement resonances by photoionizing Xe inside a $C_{60}{}^+$molecular cage *Phys. Rev.* A **88** 053402
[5] Dolmatov V K 2009 Photoionization of atoms encaged in spherical fullerenes *Theory of Confined Quantum Systems: Part Two* (Advances in Quantum Chemistry vol 58) ed J R Sabin and E Braendas (New York: Academic) pp 13–68
[6] Chakraborty H S and Magrakvelidze M 2015 Many-electron response of gas-phase fullerene materials to ultraviolet and soft x-ray photons *From Atomic to Mesoscale: The Role of Quantum Coherence in Systems of Various Complexities* ed S Malinovskaya and I Novikova (Singapore: World Scientific) p 221
[7] Harneit W, Boehme C, Schaefer S, Huebner K, Fortiropoulos K and Lips K 2007 Room temperature electronic detection of spin coherence in C_{60} *Phys. Rev. Lett.* **98** 216601
[8] Ju C, Suter D and Du J 2011 An endohedral fullerene-based nuclear spin quantum computer *Phys. Lett.* A **375** 1441
[9] Takeda A *et al* 2006 Superconductivity of doped $Ar@C_{60}$ *Chem. Commun.* **8** 912
[10] Melanko J B, Pearce M E and Salem A K 2009 *Nanotechnology in Drug Delivery* ed M M de Villiers, P Aramwit and G S Kwon (New York: Springer) p 105
[11] Ross R B *et al* 2009 Endohedral fullerenes for organic photovoltaic devices *Nat. Mater.* **8** 208
[12] Becker L, Poreda R J and Bunch T E 2000 Fullerenes: an extraterrestrial carbon carrier phase for noble gases *Proc. Natl Acad. Sci. USA* **97** 2979
[13] Lawler R G 2017 Nonmetallic endofullerenes and the endohedral environment: structure, dynamics, and spin chemistry *Endohedral Fullerenes: Electron Transfer and Spin* ed A Popov (Berlin: Springer) p 229
[14] Morton J J L, Tyryshkin A M, Ardavan A, Porfyrakis K, Lyon S A and Briggs G A D 2007 Environmental effects on electron spin relaxation in $N@C_{60}$ *Phys. Rev.* B **76** 085418
[15] Knapp C, Weiden N, Kass H, Dinse K-P, Pietzak B, Waiblinger M and Weidinger A 1998 Electron paramagnetic resonance study of atomic phosphorus encapsulated in [60]fullerene *Mol. Phys.* **95** 999
[16] Donzelli O, Briere T and Das T P 1996 Location of muonium and hydrogen in C_{60} fullerene and associated electronic structure and hyperfine properties *Hyperfine Interact.* **97** 19
[17] Chakraborty H S, Madjet M E, Renger T, Rost J-M and Manson S T 2009 Photoionization of hybrid states in endohedral fullerenes *Phys. Rev.* A **79** 061201

[18] Madjet M E, Renger T, Hopper D E, McCune M A, Chakraborty H S, Rost J-M and Manson S T 2010 Photoionization of Xe inside C_{60}: atom–fullerene hybridization, giant cross-section enhancement, and correlation confinement resonances *Phys. Rev.* A **81** 013202

[19] Maser J N, Javani M H, De R, Madjet M E, Chakraborty H S and Manson S T 2012 Atom–fullerene hybrid photoionization mediated by coupled d states in $Zn@C_{60}$ *Phys. Rev.* A **86** 053201

[20] Javani M H, De R, Madjet M E, Manson S T and Chakraborty H S 2014 Photoionization of bonding and antibonding-type atom–fullerene hybrid states in $Cd@C_{60}$ vs $Zn@C_{60}$ *J. Phys. B: At. Mol. Opt. Phys.* B **47** 175102

[21] Javani M H, Wise J B, De R, Madjet M E, Manson S T and Chakraborty H S 2014 Resonant Auger-intercoulombic hybridized decay in the photoionization of endohedral fullerenes *Phys. Rev.* A **89** 063420

[22] Dolmatov V K, Cooper M B and Hunter M E 2014 Electron elastic scattering off endohedral fullerenes $A@C_{60}$: the initial insight *J. Phys. B: At. Mol. Opt. Phys.* B **47** 115002

[23] Zhu L, Wang S, Li Y, Zhang Z, Hou H and Qin Q 1994 Evidence for fullerene with single chlorine anion inside *Appl. Phys. Lett.* **66** 702

[24] Ravinder P and Subramanian V 2011 Studies on the encapsulation of various anions in different fullerenes using density functional theory calculations and Born–Oppenheimer molecular dynamics simulation *J. Phys. Chem.* A **115** 11723

[25] Dolmatov V K and Manson S T 2010 Interior static polarization effect in $A@C_{60}$ photoionization *Phys. Rev.* A **82** 023422

[26] Baltenkov A S, Dolmatov V K, Manson S T, Msezane A Z and Pikhut V A 2003 Trends in near-threshold photoionization of off-the-center endohedral atoms *Phys. Rev.* A **68** 043202

[27] Van Leeuwen R and Baerends E J 1994 Exchange–correlation potential with correct asymptotic behavior *Phys. Rev.* A **49** 2421

[28] Rüdel A, Hentges R, Chakraborty H S, Madjet M E and Rost J M 2002 Imaging delocalized electron clouds: photoionization of C_{60} in Fourier reciprocal space *Phys. Rev. Lett.* **89** 125503

[29] Choi J, Chang E H, Anstine D M, Madjet M E and Chakraborty H S 2017 Effects of exchange-correlation potentials on the density-functional description of C_{60} versus C_{240} *Phys. Rev.* A **95** 023404

[30] de Vries J, Steger H, Kamke B, Menzel C, Weisser B, Kamke W and Hertel I V 1992 Single-photon ionization of C_{60}- and C_{70}-fullerene with synchrotron radiation: determination of the ionization potential of C_{60} *Chem. Phys. Lett.* **188** 159

[31] Miyasita1 M, Higuchi K and Higuchi M 2011 A scheme for calculating atomic structures beyond the spherical approximation *J. Mod. Phys.* **2** 421

[32] Anderson L N, Bele'en Oviedo M and Wong B M 2017 Accurate electron affinities and orbital energies of anions from a nonempirically tuned range-separated density functional theory approach *J. Chem. Theory Comput.* **13** 1656

[33] Kramida A, Ralchenko Y U, Reader J and NIST ASD Team 2019 *NIST Atomic Spectra Database ver. 5.7.1*

[34] Berzinsh U, Gustafsson M, Hanstorp D, Klinkmüller A, Ljungblad U and Martensson-Pendrill A-M 1995 Isotope shift in the electron affinity of chlorine *Phys. Rev.* A **51** 231

[35] Madjet M E, Chakraborty H S, Rost J M and Manson S T 2008 Photoionization of C_{60}: a model study *J. Phys.* B **41** 105101

[36] Madjet M E, Chakraborty H S and Manson S T 2007 Giant enhancement in low energy photoemission of Ar confined in C_{60} *Phys. Rev. Lett.* **99** 243003

[37] Javani M H, Chakraborty H S and Manson S T 2014 Valence photoionization of noble-gas atoms confined in the fullerene C_{60} *Phys. Rev.* A **89** 053402

[38] Dixit G, Chakraborty H S and Madjet M E 2013 Time delay in the recoiling valence photoemission of Ar endohedrally confined in C_{60} *Phys. Rev. Lett.* **111** 203003

[39] Connerade J-P, Dolmatov V K and Manson S T 2000 On the nature and origin of confinement resonances *J. Phys.* B **33** 2279

[40] McCune M A, Madjet M E and Chakraborty H S 2009 Reflective and collateral photoionization of an atom inside a fullerene: confinement geometry from reciprocal spectra *Phys. Rev.* A **80** 011201

[41] McCune M A, Madjet M E and Chakraborty H S 2008 Unique role of orbital angular momentum in subshell-resolved photoionization of C_{60} *J. Phys. B: At. Mol. Opt. Phys.* B **41** 201003